Integrated Sliding Mode Velocity Control of Linear Permanent Magnet Synchronous Motor with Thrust Ripple Compensation

Cong Bai, Zhonggang Yin, *Member*, *IEEE*, Jing Liu, Yanqing Zhang, and Xiangdong Sun

***Abstract* —In this paper, a compound sliding mode velocity control scheme with a new exponential reaching law (NERL) with thrust ripple observation strategy is proposed to obtain a high performance velocity loop of the linear permanent magnet synchronous motor (LPMSM) control system. A sliding mode velocity controller based on NERL is firstly discussed to restrain chattering of the conventional exponential reaching law (CERL). Furthermore, the unavoidable thrust ripple caused by the special structure of linear motor will bring about velocity fluctuation and reduced control performance. Thus, a thrust ripple compensation strategy on the basis of extend Kalman filter (EKF) theory is proposed. The estimated thrust ripple will be introduced into the sliding mode velocity controller to optimize the control accuracy and robustness. The effectiveness of the proposal is validated with experimental results.**

***Index Terms* —Linear permanent magnet synchronous motor (LPMSM), Sliding mode velocity control, New exponential reaching law, Thrust ripple compensation.**

NOMENCLATURE

u_d, u_q	*dq*-axis stator voltages, V.
i_d, i_q	*dq*-axis stator currents, A.
L_d , L_q	*dq*-axis inductances, H.
R_s	Stator resistance, Ω.
v	Mover velocity, *m*/*s*.
τ	Pole pitch, *m*.
ψ_f	PM flux linkage, Wb.
n_p	Pole pairs.
F_e	Electromagnetic thrust, N.
F_r	Thrust ripple, N.
m	mover mass, Kg.

I. INTRODUCTION

WITH the rapid progress of high-speed machining and magnetic levitation technology, linear motor has become a research hotspot [1], among which linear permanent magnet synchronous motor (LPMSM) have received extensive attention owing to its good controllability and high thrust density [2], [3]. Nowadays, LPMSM has extensive use in 3C products manufacturing and completesets of equipment, high-speed logistics and cordless elevators [4]-[6].

To achieve precise control of LPMSM drives, the velocity loop and current loop should track the command values in real time and resist disturbances effectively. Since the current loop tracking performance is only related to motor parameters, the output voltage is often calculated by the precise mathematical model to achieve good current tracking performance. However, due to the problems of strong coupling, strong nonlinearity and susceptibility to interference, the control system should have a velocity control strategy with high decoupling and strong robustness.

In a word, high-performance velocity control is very important to obtain precise control of LPMSM drives. At present, common velocity loop control methods mainly include PI control [7]-[9], internal model control (IMC) [10], [11], active disturbance rejection control (ADRC) [12], [13], intelligent control [14] and sliding mode control (SMC) [15], [16]. However, the proportional integral coefficient does not change once it is set. When the external disturbance occurs suddenly, the system cannot quickly restore the equilibrium and stable state. Since IMC has only one tunable parameter, and the dynamic and robust performance of the system would be compromised. The active disturbance rejection control has many parameters, thus these parameters are difficult to adjust to optimal value. The intelligent control has the shortcomings such as large calculation and high hardware requirements. Among these methods, SMC is famous for its perfect dynamic response, strong robustness in various working conditions.

Because of the simple structure and reliable control performance, SMC has extensive use in various fields [17]–[19], especially motor control [20]. The implementation of the SMC is divided into two stages: reaching stage and sliding mode stage. Reaching law describes the convergence trajectory of system state, which largely determines system's steady and transient performance. However, major weakness of SMC is chattering caused by discontinuous part existing in the input. Therefore, some chattering suppression methods have been proposed by scholars, such as fractional-order sliding-mode [21], nonsingular terminal SMC [22], high-order SMC [23] and reaching law method [24]. The reaching law method acts on the

Manuscript received April 01, 2022; accepted June 20, 2022. Date of publication March 25, 2023; Date of current version January 11, 2023.

This work was supported in part by National Natural Science Foundation of China (52177194), in part by State Key Laboratory of Large Electric Drive System and Equipment Technology (SKLLDJ012016006), in part by Key Research and Development Project of ShaanXi Province (2019GY-060), and in part by Key Laboratory of Industrial Automation in ShaanXi Province (SLGPT2019KF01-12) *(Corresponding Author: Zhonggang Yin)*

C. Bai, Z. Yin, Y. Zhang, X. Sun are with the Department of Electrical Engineering, Xi'an University of Technology, Xi'an, 710048, China (e-mail: 1190313031@stu.xaut.edu.cn; zhgyin@xaut.edu.cn; zhangyanqing@xaut.edu.cn; sxd1030@xaut.edu.cn).

J. Liu is with the Department of Electronic Engineering, Xi'an University of Technology, Xi'an, 710048, China (e-mail: jingliu@xaut.edu.cn).

Digital Object Identifier 10.30941/CESTEMS.2023.00003

reaching process of the sliding mode control. Therefore, it could suppress chattering more effectively. In [17], a non-switching type reaching law is presented to get faster convergence and improve dynamic performance. A new exponential reaching law is revealed in [25] to diminish chattering phenomenon. However, these reaching laws lead to a decrease in the robustness and an increase in the reaching time of the sliding mode controller.

In addition, LPMSM is the transmission mechanism of precision motion system. The quality of its output thrust directly determines the control accuracy of the system. However, when the LPMSM outputs effective electromagnetic thrust, due to the special structure and other problems, it inevitably brings vibration and thrust fluctuation with the motor position, which will reduce the thrust accuracy and even cause mechanical damage of the motor. At the same time, the velocity fluctuations caused by various periodic disturbances including the magnetic flux harmonics and cogging force will reduce system's control performance and limit applications of LPMSM in sophisticated manufacturing. Therefore, it is crucial to suppress the velocity fluctuation.

Scholars have carried out a lot of research on velocity ripple suppression methods, mainly include structural optimization and control methods [26]. Many studies focus on structural optimization through adjusting the size of some crucial structures or modifying relevant structures. However, these methods not only increase the complexity of theoretical analysis, but also increase the processing cost. Besides, the control methods are flexible and convenient, so different types of suppression methods have been studied. In [27], a periodic adaptive compensation algorithm is applied to the suppression of the cogging force and coulomb friction of the PMLM control system. However, this method has high complexity and high requirements for system hardware. [28] advances an adaptive disturbance observer to suppress periodic disturbances. However, the observer has high complexity and large amount of calculation. A torque ripple suppression method based on fractional delay variable frequency technology for PMSMs is proposed in [29], but it cost much time to reach a steady state.

A thrust ripple observation method is revealed based on the extend Kalman filter (EKF) theory. The observed thrust ripple is equivalent to thrust current and then compensated to the feedforward link, so as to suppress the thrust ripple of the LPMSM control system. Then, a compound control system that combines the improved sliding mode velocity regulator with thrust ripple compensation is proposed. The main innovations are as follows:

1) For suppressing the chattering of the CERL-SMC and reduce the reaching time, a NERL is presented, which could not only reduce the sliding-mode chattering problem, but increase the convergence rate.
2) The velocity perturbation and vibration cause by thrust ripple will increase the amplitude of discontinuities and aggravates chattering in the sliding mode control, thus a thrust ripple observation strategy is presented to estimate the thrust ripple based on the extend Kalman filter theory.
3) A compound method that combines the improved sliding mode velocity controller and the thrust ripple compensation method is developed to further enhance the LPMSM velocity loop control performance.

The remainder of this paper is organized as follows. The LPMSM control system is briefly presented in Section II. A velocity regulation scheme based on NERL-SMC is designed in Section III, and design the extended Kalman filter-based thrust ripple suppression method is proposed in Section IV. Experiments are conducted in Section V. Conclusion is drawn in Section VI.

II. LPMSM Control System

A. System Description

Block diagram of LPMSM drive is shown in Fig. 1. Generally, a high performance LPMSM control system is composed of the velocity loop and current loop. As the outer part, the velocity loop is significant important in drive system. The velocity regulation scheme has to consider various influences, such as decoupling and robustness. Therefore, the control system should have a velocity control strategy with high decoupling and strong robustness to realize the precise control. The original current command is given by the velocity controller. Through the improved sliding mode controller, the voltage command is achieved by conventional PI current controller. Then, a thrust ripple compensation strategy is designed for rejecting and compensating the thrust ripple.

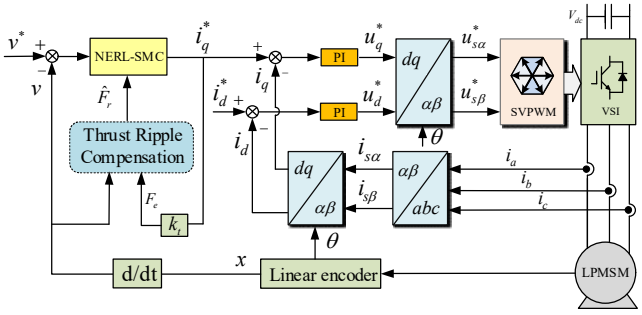

Fig. 1. Block diagram of the proposed control method.

B. Modeling of the LPMSM

The modeling of the LPMSM [2] is shown in (1), when the armature reaction, eddy current effect and hysteresis of the LPMSM are ignored, the model can be described in *dq* coordinate system as,

$$\begin{cases} u_d = R_s i_d + L_d \dfrac{di_d}{dt} - \dfrac{\pi}{\tau} v L_q i_q \\ u_q = R_s i_q + L_q \dfrac{di_q}{dt} + \dfrac{\pi}{\tau} v (L_d i_d + \psi_f) \end{cases} . \tag{1}$$

Thrust force $\vec{F}$ is expressed as [5],

$$\vec{F} = \int V \vec{f}\, dV = \oint s[(\vec{B}\cdot\vec{n})\vec{H} - \frac{1}{2}BH\vec{n}]\, dS \tag{2}$$

where S is any closed curve around this area, V is the volume in any given area, $\vec{f}$ is the force density, $\vec{n}$ is the unit normal vector, and $\vec{B}$ is the magnetic flux density, which can be expressed as,

$$\vec{B}=B_x n_x + B_y n_y. \tag{3}$$

Thereby, the thrust force $\vec{F}$ is deduced as,

$$F=\frac{1}{2\mu_0}\int_S [n_x(B_x^2 - B_y^2) + 2n_y B_x B_y]\, dS. \tag{4}$$

Due to the special structure of the end breaking, the LPMSM has obvious thrust fluctuation, which further leads to velocity fluctuation and control performance degradation. The motor thrust can be expressed as the sum of electromagnetic thrust and thrust ripple, where the thrust fluctuation is denoted by F_r.

$$F=F_e + F_r. \tag{5}$$

Since the air gap of the LPMSM is relatively large, it can be considered that the inductance in dq coordinate system is approximately equal, that is, $L_d = L_q = L_s$, so the electromagnetic thrust F_e of the LPMSM is as follows,

$$F_e = \frac{3\pi n_p \psi_f}{2\tau} i_q^* \tag{6}$$

where k_t is the thrust coefficient, $k_t = (3\pi n_p \psi_f)/(2\tau)$.

Thrust ripple is motor position-dependent pulsation mainly caused by cogging force. Write it in Fourier series as,

$$F_r = \sum_{n=1}^{\infty} f_n \cos(\frac{n\pi}{\tau}x + \delta_n) \tag{7}$$

where f_n and δ_n are the amplitude and initial angle of the nth-order harmonic, respectively.

Therefore, the dynamic equation of the LPMSM is,

$$m\frac{dv}{dt} = F_e + F_r. \tag{8}$$

It can be seen from (8) that thrust ripple will bring about velocity fluctuation, and it will cause performance deterioration of LPMSM, which restricts the application of the LPMSM in precision manufacturing equipment. Therefore, the suppression and compensation technology of thrust ripple is very important for the LPMSM drive system to obtain superior performance.

III. Velocity Regulation Scheme Based on NERL-SMC

A. CERL Design and Analysis

As mentioned above, the complete SMC process contains of two parts: reaching stage and sliding mode stage. In SMC, only the state variable is required to arrive at sliding mode surface from any initial position within a limited time, while the trajectory of the switching function composed of the system state in the reaching stage is not specified. The reaching law defines the dynamic characteristic of the switching function s. According to the requirement of different scenarios, different reaching laws are used to design the system state operation trajectories in the reaching stage, which can improve the performance. The CERL is defined as follows,

$$\frac{ds}{dt} = -\gamma sgn(s) - \varepsilon s, \gamma > 0, \varepsilon > 0 \tag{9}$$

where γ and ε are the coefficients of reaching rate, s is sliding-mode surface function, $\gamma sgn(s)$ is the isokinetic reach term, and εs is the index reach term.

For (9), the isokinetic reach term $\gamma sgn(s)$ is designed so that the reaching speed is γ instead of 0 when s is close to 0. However, even though the accessibility problem is solved by adding $\gamma sgn(s)$, the parameter value will affect the speed of reaching the sliding surface, which makes a contradiction between increasing the reaching speed and reducing the chattering.

In (9), when $s > 0$, we can get that,

$$\frac{ds}{dt} = -\gamma - \varepsilon s \tag{10}$$

Integrate (9) from 0 to t, the reaching time is,

$$t^* = \frac{1}{\varepsilon}\left\{ \mathrm{In}[s(0) + \frac{\gamma}{\varepsilon}] - \mathrm{In}\frac{\gamma}{\varepsilon} \right\}. \tag{11}$$

From (11) we can see that reaching speed increases with ε. However, an excessively large ε will cause speed exceeds when approaching sliding surface and aggravate chattering. Therefore, the contradiction between reaching speed and the gain size can be solved by setting the coefficient ε as a variable.

B. The Proposed NERL-Based SMC

A NERL is revealed to diminish chattering in CERL in this section. The NERL establishes a relationship between the controller coefficient and the distance between system state and sliding mode surface, so as to achieve the purpose of reducing chattering of SMC. The NERL is designed as,

$$\frac{ds}{dt} = -\gamma |x|^{\alpha} sgn(s) - \varepsilon |s|^{\beta \cdot sgn(|s|-1)} s \tag{12}$$

where x is the state variable. $\lim_{t\to\infty}|x| = 0, \gamma > 0, \varepsilon > 0, 0 < \alpha < 1$, $0 < \beta < 1$.

According to (12) we can see that when the system is away from sliding surface, there is s>1, then $sgn(|s|-1)=1$, and the system state reaches sliding mode surface according to $\gamma|x|^{\alpha} sgn(s)$ and $\varepsilon|s|^{\beta} s$. Meanwhile, if $|s|$ diminishes, $|s|^{\beta} s$ reaches 1, $\varepsilon|s|^{\beta} s$ converges to ε. On the other hand, due to the limitation of absolute value sign function in NERL, then $sgn(|s|-1) = -1$ and reaching speed of the variable exponential term is $\varepsilon|s|^{-\beta} s$, then $\varepsilon|s|^{-\beta} s > \varepsilon|s|^{\beta} s$, which enhances the reaching speed of the variable exponential reaching law. From the above analysis, it can be seen that the reaching speed of NERL is faster than that of CERL during the reaching process, and the chattering phenomenon in CERL is effectively suppressed.

C. Chattering Analysis

The actual motor drive digital control system is a discrete system, so this section analyzes the proposed NERL from the perspective of discretization, and compares the NERL with CERL under the condition of discretization.

If the sliding-mode surface s is close to 0, the NERL in (12) can be simplified as $ds/dt \approx -\gamma|x|^{\alpha} sgn(s)$. The first order Euler discretization of the NERL is carried out and then the following equation can be obtained,

$$s(k+1)-s(k)=-\gamma sgn(s(k))T_s|x|^{\alpha} \tag{13}$$

where T_s is the sampling period.

When $s>0$, the system trajectory reaches the sliding surface, then $s(k)=0^{+}$, and in the next period there is,

$$s(k+1)=-\gamma T_s|x|^{\alpha}. \tag{14}$$

When $s<0$, the system trajectory arrives the sliding surface, then $s(k)=0^{-}$, and in the next period there is,

$$s(k+1)=\gamma T_s|x|^{\alpha}. \tag{15}$$

Then the discrete switching bandwidth of the NERL can be expressed as,

$$\Delta_{NERL}=2\gamma T_s|x|^{\alpha}. \tag{16}$$

When s is close to 0, the CERL reaching speed is determined by $\gamma sgn(s)$, and its discrete form is,

$$s'(k+1)-s'(k)=-\gamma' sgn(s'(k))T_s. \tag{17}$$

Thus, the discrete switching bandwidth of the CERL is,

$$\Delta_{CERL}=2\gamma' T_s. \tag{18}$$

Fig. 2(a) shows the state trajectory of CERL, from which we can see that the switching bandwidth of CERL is a fixed value, and it is difficult to reach the equilibrium origin (0,0) stably, there will be chattering between ($-\gamma' T_s$, $\gamma' T_s$). In Fig. 2 (b), the power term of the state variable introduced in (16) can make the system stably converge to the equilibrium origin (0, 0), so as to effectively suppress the chattering phenomenon.

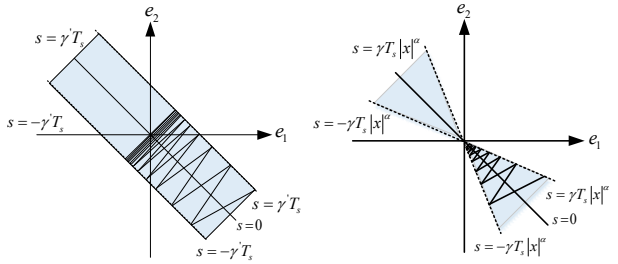

(a) (b)

Fig. 2. State trajectory comparison. (a) CERL (b) NERL

D. NERL-SMC Design

The LPMSM state variables are,

$$e_1=v^{*}-v \tag{19}$$

$$e_2=\int_{-\infty}^{t}(v^{*}-v)dt \tag{20}$$

where v^{*} is the mover velocity command value. To enhance system's dynamic response, the integral structure of the state variable is added to the sliding surface design. The sliding surface s is designed as,

$$s=e_1+ce_2,\ c>0 \tag{21}$$

where c is a constant.

Selected the velocity tracking error $x=e_1$ as the state variable, which is the difference between velocity command value and feedback value. Combining the NERL (12) with (19), (20) and (21), the output of the NERL-SMC controller can be expressed as,

$$i_q^{*}=\frac{m}{k_t}[\dot{v}^{*}+\frac{1}{m}\hat{F}_r+ce_1+\gamma|x|^{\alpha}\ sgn(s)+\varepsilon|s|^{\beta\cdot sgn(|s|-1)}\ s] \tag{22}$$

According to the above description, Fig. 3 shows the block diagram of the NERL-SMC.

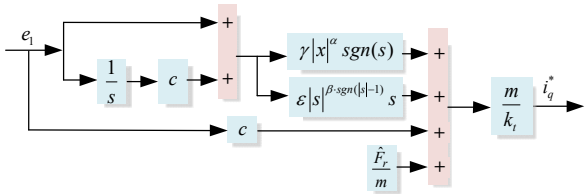

Fig. 3. Block diagram of the NERL-SMC.

E. Stability Proof

For proving the stability of NERL-SMC, the Lyapunov function is selected as,

$$V=s^2/2,\ s\neq 0. \tag{23}$$

Then, we can obtain that,

$$\begin{aligned}\dot{V}&=s\dot{s}=s[-\gamma|x|^{\alpha}\ sgn(s)-\varepsilon|s|^{\beta\cdot sgn(|s|-1)}\ s]\\&=-s[\gamma|x|^{\alpha}\ sgn(s)+\varepsilon|s|^{\beta\cdot sgn(|s|-1)}\ s]\le 0.\end{aligned} \tag{24}$$

Since the accessibility condition of SMC is $s\dot{s}<0$, then $\dot{V}(x)<0$. According to the Lyapunov stability theory, it can be concluded that the NERL-SMC velocity controller is asymptotical stable.

When the state variables arrive at the sliding mode surface, there is,

$$s=e_1+ce_2=\dot{e}_2+ce_2=0. \tag{25}$$

Solving the homogeneous linear differential equation of one variable, we can obtained that,

$$e_2=v^{*}-v=c_0e^{-\frac{t}{c}} \tag{26}$$

where c_0 is a constant. With t increases, e_2 exponentially approaches zero, which enables overshoot-free tracking.

Through the above reaching law, the contradiction between the reaching time and chattering in SMC with traditional exponential reaching law is solved. However, there are still some problems in the motion of linear motor, such as the thrust ripple. The thrust ripple directly results in the velocity fluctuation, which will deteriorate the control performance of LPMSM. Therefore, to improve the velocity regulation performance, it is necessary to identify the thrust ripple accurately. Therefore, a thrust ripple observer with extended Kalman filter is designed in the next section, and thrust ripple is observed online and then the feed-forward compensation is carried out.

IV. Design Of The Thrust Ripple Observer Baed on EKF Theory

In this section, based on the EKF principle and combined with the basic characteristics of the LPMSM, a thrust ripple observer is designed, which enables the system to estimate the thrust ripple, and update it to the controller and compensate the estimation results to the forward channel, so as to restrain the velocity fluctuation and enhance the control precision of the

LPMSM drive system.

A. Principle of EKF

1) Linear Kalman Filter

For linear systems with the following equation of state,

$$x_k = \Phi_k x_{k-1} + \Gamma_k v_k \tag{27}$$

$$y_k = H_k x_k + w_k \tag{28}$$

where x_k is the discrete state variables, Φ_k is the state matrix of discrete system, Γ_k is the system noise driven array, H_k is the output matrix, v_k and w_k are system noise and measurement noise and they satisfy the following assumptions,

$$\mathrm{cov}(v_k, v_i) = E\{v_k v_i^{\mathrm{T}}\} = \begin{cases} Q_k, i = k \\ 0, i \neq k \end{cases} \tag{29}$$

$$\mathrm{cov}(w_k, w_i) = E\{w_k w_i^{\mathrm{T}}\} = \begin{cases} R_k, i = k \\ 0, i \neq k \end{cases} \tag{30}$$

$$\mathrm{cov}(w_k, v_i) = E\{w_k v_i^{\mathrm{T}}\} = 0, \text{ arbitrary } i \text{ and } k \tag{31}$$

where $\boldsymbol{Q}_k$ and $\boldsymbol{R}_k$ are the time varying covariance matrix of system noise and measurement noise, respectively. Based on the above assumptions, the linear Kalman filter can be expressed as the follows:

1) State prediction

$$\bar{x}_k = \Phi_k \hat{x}_{k\text{-}1} \tag{32}$$

2) Modified state prediction

$$\hat{x}_k = \bar{x}_k + K_k(y_k - H_k \bar{x}_k) \tag{33}$$

3) Calculate the filter gain

$$K_k = \bar{P}_k H_k^{\mathrm{T}} (H_k \bar{P}_k H_k^{\mathrm{T}} + R_k)^{\text{-}1} \tag{34}$$

4) Calculate error covariance of prediction state

$$\bar{P}_k = \Phi_k \hat{P}_{k\text{-}1} \Phi_k^{\mathrm{T}} + \Gamma_k Q_k \Gamma_k^{\mathrm{T}} \tag{35}$$

5) Corrected prediction state error covariance

$$\hat{P}_k = (I - K_k H_k)\bar{P}_k \tag{36}$$

Fig. 4 shows the calculation flow of the linear Kalman filter algorithm, which is composed of state calculation loop and gain calculation loop. The online estimation methods based on Kalman filter are all based on this framework, while the calculation methods of the state update and the gain matrix update are different.

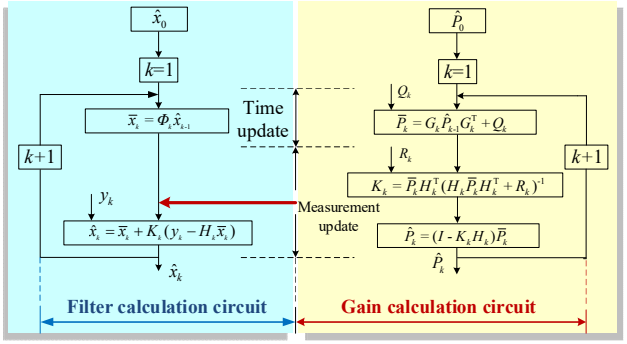

Fig. 4. Flow of Kalman Filter Algorithm.

2) Extended Kalman Filter

Suppose the nonlinear system model is as follows,

$$x_k = f(x_{k-1}, u_k, v_k) \tag{37}$$

$$y_k = h(x_k, w_k) \tag{38}$$

where, u_k is the control variable; y_k is the measurement variable, $f(\bullet)$ is a nonlinear system function, $h(\bullet)$ is a nonlinear observation function.

At time k, the nonlinear system function is linearized near the working point, then we can obtain,

$$\begin{aligned} x_k &= f(x_{k-1}, u_k, v_k) = f(\hat{x}_{k-1} + \Delta x, u_k, 0 + \Delta w) \\ &\approx f(\hat{x}_{k-1}, u_k, 0) + \frac{\partial f}{\partial x}(x_{k-1}, u_k, v_k)\Big|_{(\hat{x}_{k-1}, u_k, 0)} \Delta x \\ &+ \frac{1}{2!}\frac{\partial^2 f}{\partial x^2}(x_{k-1}, u_k, v_k)\Big|_{(\hat{x}_{k-1}, u_k, 0)} \Delta x^2 \\ &+ \frac{1}{3!}\frac{\partial^2 f}{\partial x^2}(x_{k-1}, u_k, v_k)\Big|_{(\hat{x}_{k-1}, u_k, 0)} \Delta x^3 + \cdots \\ &+ \frac{\partial f}{\partial v}(x_{k-1}, u_k, v_k)\Big|_{(\hat{x}_{k-1}, u_k, 0)} \Delta v \\ &+ \frac{1}{2!}\frac{\partial^2 f}{\partial v^2}(x_{k-1}, u_k, v_k)\Big|_{(\hat{x}_{k-1}, u_k, 0)} \Delta v^2 \\ &+ \frac{1}{3!}\frac{\partial^2 f}{\partial v^2}(x_{k-1}, u_k, v_k)\Big|_{(\hat{x}_{k-1}, u_k, 0)} \Delta v^3 + \cdots \end{aligned} \tag{39}$$

Ignoring the higher-order terms, formula (39) becomes,

$$\begin{aligned} x_k &= f(x_{k-1}, u_k, v_k) = f(\hat{x}_{k-1} + \Delta x, u_k, 0 + \Delta v) \\ &\approx f(\hat{x}_{k-1}, u_k, 0) + \frac{\partial f}{\partial x}(x_{k-1}, u_k, v_k)\Big|_{(\hat{x}_{k-1}, u_k, 0)} \Delta x \\ &+ \frac{\partial f}{\partial v}(x_{k-1}, u_k, v_k)\Big|_{(\hat{x}_{k-1}, u_{k-1}, 0)} \Delta v \end{aligned} \tag{40}$$

Define the following expression,

$$f(\hat{x}_{k-1}, u_{k-1}, 0) = \bar{x}_k, G_k = \frac{\partial f}{\partial x}(\hat{x}_{k-1}, u_k, v_k) = \bar{x}_k\Big|_{(\hat{x}_{k-1}, u_k, 0)},$$

$$V_k = \frac{\partial f}{\partial x}(\hat{x}_{k-1}, u_k, v_k)) = \bar{x}_k\Big|_{(\hat{x}_{k-1}, u_k, 0)}.$$

(39) can be rewritten as,

$$x_k = f(\hat{x}_{k-1}, u_k, v_k) \approx \bar{x}_k + G_k(x_{k-1} - \hat{x}_{k-1}) + V_k v_k \tag{41}$$

Similarly, if $(\bar{x}_k, 0)$ is regarded as the current working point of $h(\cdot)$, then multidimensional Taylor expansion is carried out.

$$\begin{aligned} y_k &= h(x_k, w_k) = h(\bar{x}_k + \Delta x, 0 + w_k) \\ &\approx h(\bar{x}_k, 0) + \frac{\partial h}{\partial x}(x_k, w_k)\Big|_{(\bar{x}_k, 0)} \Delta x + \frac{1}{2!}\frac{\partial^2 h}{\partial x^2}(x_k, w_k)\Big|_{(\bar{x}_k, 0)} \Delta x^2 \\ &+ \frac{1}{3!}\frac{\partial^3 h}{\partial w^3}(x_k, w_k)\Big|_{(\bar{x}_k, 0)} \Delta x^3 + \cdots + \frac{\partial h}{\partial w}(x_k, w_k)\Big|_{(\bar{x}_k, 0)} \Delta w \\ &+ \frac{1}{2!}\frac{\partial^2 h}{\partial w^2}(x_k, w_k)\Big|_{(\bar{x}_k, 0)} \Delta w^2 + \frac{1}{3!}\frac{\partial^3 h}{\partial w^3}(x_k, w_k)\Big|_{(\bar{x}_k, 0)} \Delta w^3 + \cdots \end{aligned} \tag{42}$$

Define $W_k = \frac{\partial h}{\partial v}(x_k, w_k)\Big|_{(\bar{x}_k, 0)}$, $L_k = \frac{\partial h}{\partial x}(x_k, w_k)\Big|_{(\bar{x}_k, 0)}$, $h(\bar{x}_k, 0) = \bar{y}_k$, after omitting the high-order terms, (42) is written as follows,

$$y_k = h(x_k, w_k) \approx \bar{y}_k + L_k(x_k - \hat{x}_k) + W_k w_k \tag{43}$$

Through the above derivation, the state estimation problem

of nonlinear system is transformed into a linear system problem. The EKF algorithm is obtained by using the calculation method of classical linear Kalman filter framework.

B. Design of the Thrust Ripple Observer of the LPMSM

The dynamic equation of the LPMSM is expressed in (8). The discrete state space model of LPMSM is as follows,

$$\begin{cases} \boldsymbol{x}(k+1) = f[\boldsymbol{x}(k), \boldsymbol{x}(k)] + \boldsymbol{w}(k) \\ \boldsymbol{y}(k) = \boldsymbol{h}[\boldsymbol{x}(k)] + \boldsymbol{v}(k) \end{cases} \tag{44}$$

Based on the mechanical motion equation of the LPMSM, the thrust ripple compensation scheme based on EKF is established. The state variables are selected as $\boldsymbol{x} = [v \ \hat{F}_r]^{\mathrm{T}}$ .The algorithm process is as follows:

(1) Initialization of state variables

$$\hat{\boldsymbol{x}}_0 = \boldsymbol{E}[\boldsymbol{x}_0] \tag{45}$$

$$\boldsymbol{P}_0 = \boldsymbol{E}[(\boldsymbol{x}_0 - \hat{\boldsymbol{x}}_0)(\boldsymbol{x}_0 - \hat{\boldsymbol{x}}_0)^{\mathrm{T}}] \tag{46}$$

where $\boldsymbol{x}_0$ is the initial value of the state variable and $\boldsymbol{P}_0$ is the initial value of the error covariance matrix.

(2) Calculate Jacobian matrix $\boldsymbol{G}$ and $\boldsymbol{H}$

$$\boldsymbol{G}_k = \frac{\partial}{\partial \boldsymbol{x}}(\boldsymbol{A}_{k-1}\boldsymbol{x} + \boldsymbol{B}_{k-1}u)\Big|_{x=\bar{x}_k} = \begin{pmatrix} 1 & [u_{k-1} - F_r]T_s \\ 0 & 1 \end{pmatrix} \tag{47}$$

$$\boldsymbol{H}_k = \frac{\partial}{\partial x}(\boldsymbol{C}_{k-1}\boldsymbol{x})\Big|_{x=\bar{x}_k} = \begin{pmatrix} 1 & 0 \end{pmatrix} \tag{48}$$

(3)One step prediction of the state variables

$$\bar{\boldsymbol{x}}_{k/k} = f(\hat{\boldsymbol{x}}_{k/k-1}, u_{k-1}) \tag{49}$$

where $\hat{\boldsymbol{x}}_{k/k-1}$ is the best estimate of the previous time, $\bar{\boldsymbol{x}}_{k/k}$ is the predicted value of the state variable at the current moment.

(4)Forecast the error covariance matrix

$$\bar{\boldsymbol{P}}_{k/k} = \boldsymbol{G}_k \hat{\boldsymbol{P}}_{k/k-1} \boldsymbol{G}_k^T + \boldsymbol{Q} \tag{50}$$

where $\hat{\boldsymbol{P}}_{k/k-1}$ is the error covariance matrix of the upper time, $\bar{\boldsymbol{P}}_{k/k}$ is the predicted value of the current time, $\boldsymbol{Q}$ is the system noise covariance matrix.

(5)Calculate the Kalman filter gain matrix

$$\boldsymbol{K}_k = \bar{\boldsymbol{P}}_{k/k} \boldsymbol{H}_k^T (\boldsymbol{H}_k \bar{\boldsymbol{P}}_{k/k} \boldsymbol{H}_k^T + \boldsymbol{R})^{-1} \tag{51}$$

where $\boldsymbol{K}_k$ is gain matrix of Kalman filter, $\boldsymbol{R}$ is the measurement covariance matrix of control system.

(6)Estimation of state variables

$$\hat{\boldsymbol{x}}_{k/k} = \bar{\boldsymbol{x}}_{k/k} + \boldsymbol{K}_k (y_k - \boldsymbol{g}(\bar{\boldsymbol{x}}_{k/k}, u_k)) \tag{52}$$

where y_k is the actual output, $\boldsymbol{g}(\bar{\boldsymbol{x}}_{k/k}, u_k)$ is the predicted value of the output.

The Kalman filter gain matrix $\boldsymbol{K}_k$ is used as the coefficient of the difference between y_k and $\boldsymbol{g}(\bar{\boldsymbol{x}}_{k/k}, u_k)$, so as to modify the predicted value of the state variable, and finally obtain the best estimated value $\hat{\boldsymbol{x}}_{k/k}$ of the state variable.

(7)Covariance matrix of state variable estimation error

$$\hat{\boldsymbol{P}}_{k/k} = (\boldsymbol{I} - \boldsymbol{K}_k \boldsymbol{H}_k) \bar{\boldsymbol{P}}_{k/k} \tag{53}$$

where $\boldsymbol{I}$ is the identity matrix. Through $\boldsymbol{K}_k$ to modify the current time $\bar{\boldsymbol{P}}_{k/k}$, the best estimate of $\bar{\boldsymbol{P}}_{k/k}$ is obtained. Fig. 5 shows the block diagram of the thrust ripple estimation.

V. Experimental Results

To verify the validity of the proposal, experiments based on one LPMSM system are conducted. Parameters of the studied LPMSM are listed in Table I. Fig. 6 indicates the block diagram of the experimental setup, which is a dual closed-loop system contains a velocity outer loop and two current inner loops. The velocity loop is the key factor for obtaining good velocity control performance. Thus, the proposed scheme to achieve superior velocity control is obtained. The PI controller is adopted as the automatic current regulator (ACR), and a cascade structure combined with a NERL-based SMC velocity controller is formed. An EKF-based thrust ripple estimator is designed to estimate and compensate the thrust ripple.

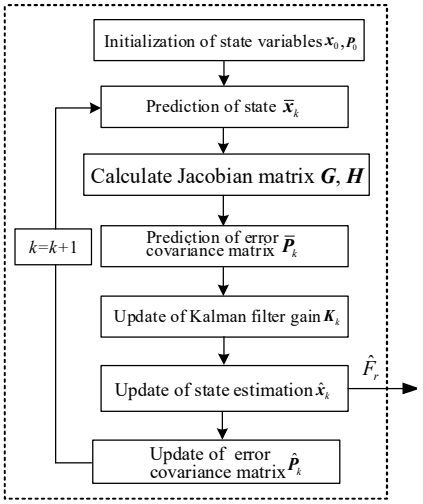

Fig. 5. Block diagram of thrust ripple estimation based on the EKF.

TABLE I
PARAMETERS OF THE LPMSM.

Parameter	Value	Unit
Pole pitch	15	mm
PM flux linkage	0.2	Wb
Thrust constant	48.6	N/A
Mover mass	0.7	kg
Stator resistance	8.4	Ω
Stator inductance	37.1	mH

The experimental setup of the LPMSM is shown in Fig. 7. The testing setup consists of one main circuit, one DSP control board, one linear encoder, and some other tools, and the core controller is a DSP TMS320F28335 of TI company. The

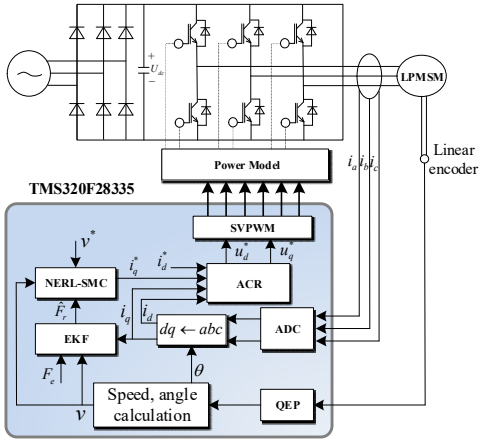

Fig. 6. Block diagram of the experimental bench.

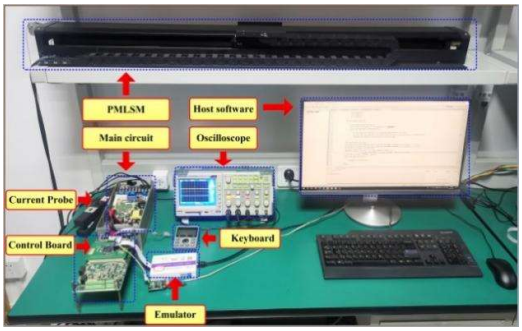

Fig. 7. Photograph of the experimental setup.

sampling frequency of control system is 8 kHz. The proposed algorithm is written by C language in CCS6.0.

The software flow of the LPMSL control system mainly consists of initialization program, main function program, PWM interrupt program, current polarity detection program, etc. The PWM interrupt cycle is 125μs, which mainly completes coordinate transformation, thrust ripple estimation algorithm, SVPWM generation, dead time compensation and other functions. Fig.8 (a) and Fig.8 (b) show the flow charts of the PWM interruption and thrust ripple estimation, respectively.

To fully verify the validity of the proposal, the performance of the proposal has been carried out under these cases: 1) overall performance of the proposed method; 2) validity verification of the NERL-SMC; 3) thrust ripple compensation.

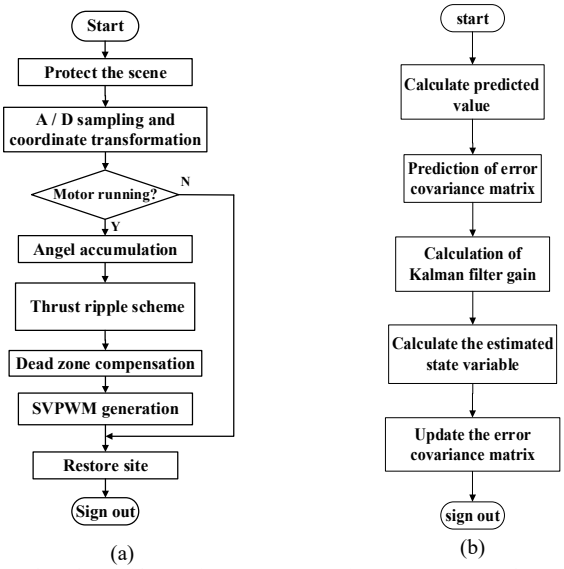

Fig. 8. Flowchart of key software. (a) PWM interrupt program (b) EKF-based thrust ripple estimation method subprogram

A. Overall Performance Verification

When the tested motor starting from standstill to 0.45m/s, the experimental results based on the proposed compound robust sliding mode velocity control with thrust ripple estimation are shown in Fig. 9, which shows the mover velocity command value, the mover velocity feedback value, and *u*-phase current, respectively. The velocity command value increases from standstill to 0.45m/s through a ramp way, and the velocity feedback value follows the velocity command value quickly, which shows that the feedback value of the proposal can quickly track the given value, and has good control performance.

Fig. 10 presents the control performance of the proposal when the LPMSM runs from start to 0.45m/s. The waveforms are mover velocity feedback value, *q*-axis current and *u*-phase current. As seen from the experimental results, the speed feedback value has almost no overshoot and fluctuation, and the phase current has good sinusoidal degree. It shows that the proposal has good transient performance and can effectively suppress the velocity ripple caused by the thrust ripple.

Fig. 11 shows the corresponding results when the velocity reversal from -0.375m/s to 0.375m/s by using the proposed method, in which the waveforms are mover velocity command value, mover velocity feedback value, velocity error and *u*-phase current. When the LPMSM is in steady state operation, the motor decelerates from 0.375m/s to 0, and then reversely accelerates to the velocity command value quickly. From the experimental results, the velocity response of the LPMSM is fast and the current waveform has little oscillation during velocity reversal. It can be seen from Fig. 11that the proposed compound method has excellent

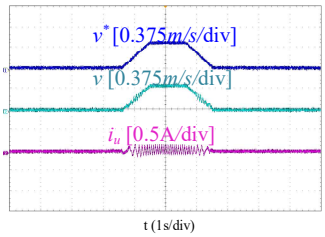

Fig. 9. Velocity and *u*-phase current response under the proposed method.

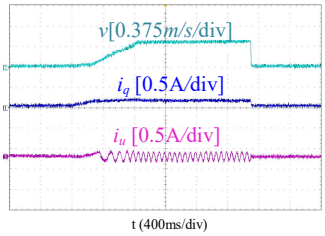

Fig.10. No-load starting response under the proposed method.

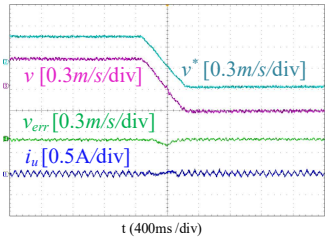

Fig. 11. Reverse response under the proposed method.

dynamic performance during the velocity reversal.

B. Validity Verification of the NERL-SMC

To verify the dynamic performance of the proposed compound method, the comparison experiments are conducted. Fig. 12(a) shows the corresponding results with the CERL-SMC method at 0.45m/s with no-load start-up, and Fig. 12(b) shows the experimental results with the NERL-SMC method at 0.45m/s with no-load start-up. From top to bottom, the mover velocity feedback value, the *q*-axis current, and the *u*-phase current are shown, respectively. As shown in Fig. 12, the overshoot and settling time of the velocity feedback value

are 4.3% and 150ms, under the CERL-SMC method, respectively. In addition, the settling time of the velocity feedback value are 85ms and the overshoot is nearly 0, under the NERL-SMC method. Besides, the fluctuation of the q-axis current under the CERL-SMC method is larger than the q-axis fluctuation of the NERL-SMC method. Therefore, the experimental waveforms show that the proposed NERL-SMC has good transient performance and improves the chattering phenomenon.

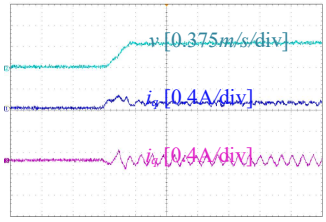

(a)

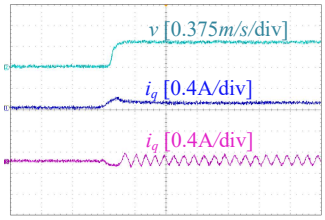

(b)

Fig.12. No-load starting response. (a) CERL-SMC (b) NERL-SMC.

In this test, the motor starts from no-load, and then the velocity reference is step changed from standstill to 0.45m/s at 0.8s. The motor operated at 0.45m/s and then back to standstill. Fig. 13 compares the corresponding results with the two sliding mode control methods with different exponential convergence laws. Fig. 13(a) shows the experimental waveforms based on the CERL-SMC method, and Fig. 13(b) shows the experimental waveforms based on the NERL-SMC method. From top to bottom, the mover velocity command value, the mover velocity feedback value, the velocity tracking error, and the u-phase current are given, respectively. The settling times of the CERL-SMC and the NERL-SMC after the sudden velocity changes are 800ms and 120ms, respectively. The corresponding results show that the proposed NERL-SMC has better dynamic performance than the CERL-SMC.

Fig. 14 shows the experimental results with the two different methods at 0.45m/s with a step load. Fig. 14 (a) and Fig. 14 (b) show the results under the CERL-SMC and NERL-SMC, respectively. The settling time of the mover velocity feedback is 220ms with the CERL-SMC method and it is 150ms with the

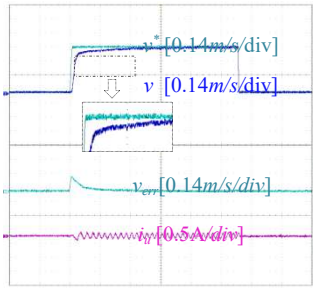

(a)

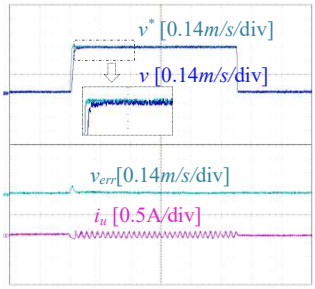

(b)

Fig. 13. Experimental results under sudden speed changes. (a) CERL-SMC (b) NERL-SMC

NERL-SMC method, respectively. The velocity drops under the NERL-SMC method is obviously smaller than that of the CERL-SMC method. In a word, compared with CERL-SMC, the proposed NERL-SMC method has better transient performance and anti-load disturbance performance.

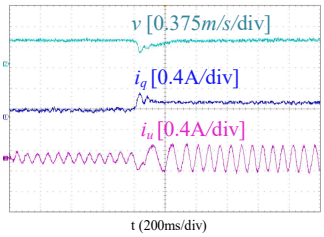

(a)

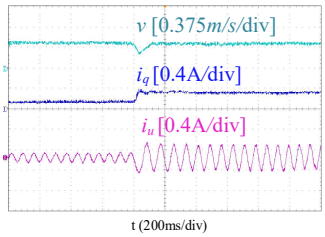

(b)

Fig. 14. Comparative results under step load. (a) CERL-SMC (b) NERL-SMC

C. *Thrust Ripple Compensation*

To better verify the validity of the thrust ripple estimation algorithm, the performance criterion to evaluate the thrust ripple is the velocity fluctuation factor (VFF), $\mathrm{VFF} = (v_{pk-pk} / v_{rated}) \times 100\%$. The velocity fluctuation factor is defined as the ratio between the peak value and the rated value of the LPMSM.

The LPMSM will inevitably generate thrust ripple due to the end disconnection. The thrust ripple will cause the motor velocity fluctuation and deteriorate the control performance, thus restricting the application of LPMSM in precision manufacturing equipment. Therefore, thrust ripple suppression is very necessary. In this part, an EKF-based observation technology is designed to estimate and compensate for thrust ripple, thereby realizing thrust ripple suppression. In the LPMSM control system, PI regulators are employed in current loops, and k_p and k_i are set to $k_p = 0.8$ and $k_i = 0.01$. The velocity controller employs the NERL-SMC method. The parameters of the SMC are $c = 300, \gamma = 20, \varepsilon = 0.01$.

Fig. 15 shows the velocity and position waveforms of

LPMSM from standstill to 0.18 m/s before and after the adoption of thrust ripple compensation method. After the acceleration stage, the velocity reaches the command value and runs stably at 0.18 m/s. As shown in Fig. 15(a), the velocity fluctuation is obvious, and the velocity feedback value fluctuates near the velocity command value. After adopting the proposed EKF-based thrust ripple compensation method, as shown in Fig. 15(b), the velocity fluctuation is significant reduced, which shows the validity of the thrust ripple compensation method. Compared with the experimental results before and after adopting the thrust fluctuation suppression method, the performance of velocity and position information after compensation is better. Fig. 15

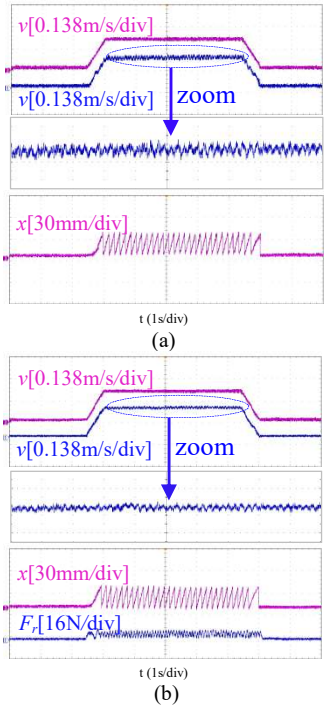

Fig. 15. Velocity tracking performance of 0.18m/s. (a) without thrust ripple estimation (b) with thrust ripple estimation

TABLE II.
COMPARISON RESULTS WITHOUT AND WITH THRUST RIPPLE COMPENSATION.

Methods	Without compensation	With compensation
VFF	2.55%	1.28%

shows the effectiveness of the proposed thrust fluctuation compensation method.

VI. CONCLUSION

A compound SMC with EKF-based thrust ripple estimation technology is proposed, which enhances the robustness and transient performance of LPMSM drive system. The NERL-based SMC could effectively reduce chattering of SMC, and enhance convergence speed as well. Then, since the thrust ripple will increase the amplitude of discontinuities and aggravates chattering in SMC, a thrust ripple estimation technology is presented to restrain the thrust ripple based on the extend Kalman filter theory. It feeds back the estimated thrust ripple to SMC with improved reaching law. Finally, the effectiveness of the proposal is validated with experimental results.

REFERENCES

[1] R. Cao, Y. Jin, M. Lu, and Z. Zhang. "Quantitative comparison of linear flux-switching permanent magnet motor with linear induction motor for electromagnetic launch system". *IEEE Transactions on Industrial Electronics*, vol. 65, no. 9, pp. 7569–7578, 2018.

[2] F. F. M. El-Sousy and K. A. Abuhasel. "Nonlinear robust optimal control via adaptive dynamic programming of permanent-magnet linear synchronous motor drive for uncertain two-axis motion control system", *IEEE Transactions on Industry Applications*, vol. 56, no. 2, pp. 1940-1952, 2020.

[3] Z. Li, S. Zhou, Y. Xiao, and L. Wang. "Sensorless vector control of permanent magnet synchronous linear motor based on self-adaptive super-twisting sliding mode controller", *IEEE Access*, pp. 1–1, 2019.

[4] Z. Jing, H. Yu, M. Hu, H. Lei, and X. Tao. "Research on a PM slotless linear generator based on magnet field analysis model for wave energy conversion", *IEEE Transactions on Magnetics*, vol. 53, no. 11, pp. 1–4, 2017.

[5] R. Yang, L. Li, M. Wang and C. Zhang. "Force ripple compensation and robust predictive current control of PMLSM using augmented generalized proportional–integral observer", *IEEE Journal of Emerging and Selected Topics in Power Electronics*, vol. 9, no. 1, pp. 302–315, 2021.

[6] F. Song, L. Yang, J. X. Xu, X. Yang, H. Ping, and Z. Yang. "Iterative learning identification and compensation of space-periodic disturbance in PMLSM systems with time delay", *IEEE Transactions on Industrial Electronics*, vol. PP, no. 99, pp. 1–1, 2017.

[7] R. Errouissi, A. Al-Durra, and S. M. Muyeen. "Experimental validation of a novel PI speed controller for ac motor drives with improved transient performances", *IEEE Transactions on Control Systems Technology*, pp. 1–8, 2017.

[8] L. Niu, D. Xu, M. Yang, X. Gui, and Z. Liu. "On-line inertia identification algorithm for PI parameters optimization in speed loop", *IEEE Transactions on Power Electronics*, vol. 30, no. 2, pp. 849–859, 2015.

[9] C. Xia, B. Ji, and Y. Yan. "Smooth speed control for low speed high-torque permanent-magnet synchronous motor using proportional–integral–resonant controller", *IEEE Transactions on Industrial Electronics*, vol. 62, no. 4, pp. 2123–2134, 2015.

[10] Q. Zhu, Z. Yin, Y. Zhang, J. Niu, Y. Li, and Y. Zhong. "Research on two-degree-of-freedom internal model control strategy for induction motor based on immune algorithm", *IEEE Transactions on Industrial Electronics*, vol. 63, no. 3, pp. 1981–1992, 2016.

[11] G. Liu, L. Chen, W. Zhao, Y. Jiang, and L. Qu. "Internal model control of permanent magnet synchronous motor using support vector machine generalized inverse", *IEEE Transactions on Industrial Informatics*, vol. 9, no. 2, pp. p.890–898, 2013.

[12] J. Li, H. Ren and Y. Zhong. "Robust speed control of induction motor drives using first-order auto-disturbance rejection controllers", *IEEE Transactions on Industry Applications*, vol. 51, no. 1, pp. 712-720, 2015.

[13] C. Du, Z. Yin, Y. Zhang, J. Liu, X. Sun, and Y. Zhong. "Research on active disturbance rejection control with parameter autotune mechanism for induction motors based on adaptive particle swarm optimization algorithm with dynamic inertia weight", *IEEE Transactions on Power Electronics*, vol. 34, no. 3, pp. 2841–2855, 2019.

[14] Z. Yin, C. Du, J. Liu, X. Sun, and Y. Zhong. "Research on auto disturbance-rejection control of induction motors based on an ant colony optimization algorithm", *IEEE Transactions on Industrial Electronics*, vol. 65, no. 4, pp. 3077–3094, 2018.

[15] Y. Wang, Y. Feng, X. Zhang, and J. Liang. "A new reaching law for antidisturbance sliding-mode control of PMSM speed regulation system", *IEEE Transactions on Power Electronics*, vol. 35, no. 4, pp. 4117–4126, 2020.

[16] M. A. M. Cheema, J. E. Fletcher, M. Farshadnia, X. Dan, and M. F. "Rahman. Combined speed and direct thrust force control of linear permanent-magnet synchronous motors with sensorless speed estimation using a sliding-mode control with integral action", *IEEE Transactions on Industrial Electronics*, vol. 64, no. 5, pp. 3489–3501, 2017.

[17] A. Bartoszewicz and P. Lesniewski. "New switching and nonswitching type reaching laws for SMC of discrete time systems", *IEEE Transactions on Control Systems Technology*, vol. 24, no. 2, pp. 670–677, 2016.

[18] Q. Xu. "Piezoelectric nanopositioning control using second-order discrete-time terminal sliding-mode strategy", *IEEE Transactions on Industrial Electronics*, vol. 62, no. 12, pp. 7738–7748, 2015.

[19] X. Zhang, H. Su, and R. Lu. "Second-order integral sliding mode control for uncertain systems with control input time delay based on singular perturbation approach", *IEEE Transactions on Automatic Control*, vol. 60, no. 11, pp. 3095–3100, 2015.

[20] Z. Yu, K. W. E. Cheng, J. Hu, S. D. Huang, and J. F. Pan. "A new decoupled Rotlin motor with fuzzy sliding mode control", *IEEE Transactions on Magnetics*, vol. 54, no. 11, pp. 1–5, 2018.

[21] G. Sun, Z. Ma, and J. Yu. "Discrete-time fractional order terminal sliding mode tracking control for linear motor", *IEEE Transactions on Industrial Electronics*, vol. PP, no. 99, pp. 1–1, 2017.

[22] W. Liu, S. Chen, and H. Huang. "Adaptive nonsingular fast terminal sliding mode control for permanent magnet synchronous motor based on disturbance observer", *IEEE Access*, vol. PP, no. 99, pp. 1–1, 2019.

[23] B. Wang, C. Luo, Y. Yu, G. Wang, and D. G. Xu. "Anti-disturbance speed control for induction machine drives using high-order fast terminal sliding-mode load torque observer", *IEEE Transactions on Power Electronics*, pp. 1–1, 2017.

[24] S. M. Mozayan, M. Saad, H. Vahedi, H. Fortin-Blanchette, and M. Soltani. "Sliding mode control of PMSG wind turbine based on enhanced exponential reaching law", *IEEE Transactions on Industrial Electronics*, vol. 63, no. 10, pp. 6148–6159, 2016.

[25] Jianwei, Leng, Chang, and Ma. "Sliding mode control for PMSM based on a novel hybrid reaching law ", in *Proc. of the 37th Chinese Control Conference*, 2018.

[26] M. Wang, L. Li and R. Yang. "Overview of thrust ripple suppression technique for linear motors", *Chinese Journal of Electrical Engineering*, vol. 2, no. 1, pp. 77-84, 2016.

[27] Hyo-Sung Ahn, YangQuan Chen and Huifang Dou. "State-periodic adaptive compensation of cogging and coulomb friction in permanent-magnet linear motors", *IEEE Transactions on Magnetics*, vol. 41, no. 1, pp. 90-98, 2005.

[28] K. Cho, J. Kim, S. B. Choi and S. Oh. "A high-precision motion control based on a periodic adaptive disturbance observer in a PMLSM", *IEEE/ASME Transactions on Mechatronics*, vol. 20, no. 5, pp. 2158-2171, 2015.

[29] M. Tang, A. Gaeta, A. Formentini and P. Zanchetta. "A fractional delay variable frequency repetitive control for torque ripple reduction in PMSMs", *IEEE Transactions on Industry Applications*, vol. 53, no. 6, pp. 5553-5562, 2017.

Cong Bai was born in Shaanxi, China, in 1993. She received the B.S. degree in Electrical Engineering from Xi'an University of Technology, Xi'an, China, in 2015. She is currently working toward the Ph.D. degree in electric machines and electric apparatus from Xi'an University of Technology, Xi'an, China. Her main field of interest is high-performance control of linear motor.

Zhonggang Yin (M'13) was born in Shandong, China, in 1982. He received the B.S., M.S. and Ph.D. degrees in Electrical Engineering from Xi'an University of Technology, Shaanxi, China, in 2003, 2006 and 2009, respectively. In 2009, he joined electrical engineering department of Xi'an University of Technology, where he is currently a professor. His research interests include high performance control of ac motor, and digital control of power converters.

Jing Liu was born in Anhui, China, in 1982. She received the B.S., M.S. and Ph.D. degrees in Electronic Engineering from Xi'an University of Technology, Shaanxi, China, in 2003, 2006 and 2009, respectively. In 2009, she joined electronic engineering department of Xi'an University of Technology, where she is currently an associate professor. Her research interests include the power semiconductor devices and their application to power electronic devices.

Yanqing Zhang received the B.S., M.S., and Ph.D. degrees in Electrical Engineering from Xi'an University of Technology, Xi'an, China, in 2012, 2015 and 2019, respectively. In 2019, he joined the Department of Electrical Engineering, Xi'an University of Technology, where he is currently a lecturer. His main field of interest is high performance control of ac motor.

Xiangdong Sun was born in Shenyang, China, in 1971. He received Ph.D. degree in Electrical Engineering from Xi'an University of Technology, Xi'an, China, in 2003. He did the postdoctoral research in Tokyo Polytechnic University supported by the government scholarship of Japan during 2006-2008.

He is currently a professor with the Department of Electrical Engineering, Xi'an University of Technology. His research interests include motor control, power electronics, and renewable energy system.